Optogenetic ion pumps differ with respect to the secondary pattern of K^+ redistribution

R. Ryley Parrish[1,2], Tom Jackson-Taylor[1], Juha Voipio[3], Andrew J. Trevelyan[1] *

1. Newcastle University Biosciences Institute, Medical School, Framlington Place, Newcastle upon Tyne, NE2 4HH, UK.
2. Department of Cell Biology and Physiology, Brigham Young University, Provo, Utah. 84602, USA.
3. Faculty of Biological and Environmental Sciences, Molecular and Integrative Biosciences, University of Helsinki, 00014 Helsinki, Finland

* Correspondence to andrew.trevelyan@ncl.ac.uk

Abbreviated title: Ionic redistribution following optogenetic pump activity.

Number of figures: 3

Number of tables: 1

Keywords: Archaerhodopsin, Halorhodopsin, chloride-cation-cotransporter, potassium, chloride.

The authors declare no conflicts of interest.

Acknowledgments: The work was supported by grants from BBSRC (BB/P019854/1) and MRC (MR/R005427/1). We would like to thank the support staff in the animal facilities at Newcastle University.

Abstract

We recently reported that strong activation of the optogenetic chloride pump, Halorhodopsin leads to a secondary redistribution of K^+ ions into the cell, through tonically open, "leak" K^+ channels. Here we show that this effect is not unique to halorhodopsin, but is also seen with activation of another electrogenic ion pump, archaerhodopsin. The two opsins differ however in the size of the rebound rise in extracellular potassium, $[K^+]_o$, after the end of activation, which is far larger with halorhodopsin than for archaerhodopsin activation. Multiple linear regression modelling indicates that most of the variance in the post-illumination surge in $[K^+]_o$ was explained by the type of opsin, and almost nothing by the size of the preceding, illumination-induced drop in $[K^+]_o$. These data provide additional support for the hypothesis that intense chloride-loading of cells, as occurs naturally following intense bursts of GABAergic synaptic bombardment, or artificially following halorhodopsin activation, is followed by extrusion of both Cl^- and K^+ coupled together. We discuss this with respect to the pattern of $[K^+]_o$ rise that occurs at the onset of seizure-like events.

Introduction

The development of optogenetics techniques and tools have presented new ways of manipulating neuronal excitability (Deisseroth, 2015), using either light activated ion channels (Boyden et al., 2005) or electrogenic ion pumps (Chow et al., 2010; Zhang et al., 2007). The real power of these remarkable tools is that they may be targeted very precisely to specific subsets of cells, or even to subcellular domains, allowing experimental control to be delivered at these sites. The induced ion movements, however, do alter the internal and external milieu, meaning that there may be unintended secondary effects both at and away from the site of expression. These, though, may be put to good use for exploring neuronal physiology and pathology, so it is worth documenting these effects.

Halorhodopsin was the first optogenetic protein to be used for inhibiting neurons, using light to drive chloride into neurons to hyperpolarize them (Zhang et al., 2007). We recently showed that this light-activated chloride movement has several interesting secondary effects (Parrish et al., 2023). Firstly, the hyperpolarization of membrane potential alters the balance between the electrical and chemical gradients for other ions; since the open "leak" channels at rest are mainly K^+ channels, there follows a redistribution of K^+ ions into expressing cells, causing the extracellular K^+ concentration, $[K^+]_o$, to drop. Consequently, there is a negative shift in membrane potential in other non-expressing neurons, with a measurable drop in their excitability (an "off-target" inhibition that may be important to recognize when interpreting optogenetic experiments). Most surprising, though, was that activation of halorhodopsin triggered cortical spreading depolarization (CSD) events that occurred even during periods of ongoing illumination, when most neurons were hyperpolarized and $[K^+]_o$ was below baseline levels. Interestingly, on the trials where CSD were not induced and once illumination ended, there was then a large rebound surge in $[K^+]_o$.

Archaerhodopsin, another commonly used inhibitory optogenetic ion pump, delivers hyperpolarization of neurons in a different way, by driving protons out of the cell (Chow et al., 2010). As such, archaerhodopsin activation should show some of the secondary effects of halorhodopsin, but not others. It has already been shown that activation of halorhodopsin, but not archaerhodopin, induces a pronounced chloride-loading of neurons that may persist for

74 many seconds (Alfonsa et al., 2015; Raimondo et al., 2012). Since Cl^- clearance is achieved
75 primarily by coupling to K^+ extrusion, through the electroneutral chloride-cation cotransporter,
76 KCC2 (Kaila et al., 2014; Rivera et al., 1999), the degree of chloride loading will influence the
77 amplitude of the post-illumination surge in $[K^+]_o$. To examine these differences, we present
78 recordings of $[K^+]_o$ in neocortical brain slices in which archaerhodopsin is expressed widely in
79 the pyramidal population, to show that it shares with halorhodopsin the effect of inducing an
80 inward movement of K^+ ions during the period of illumination. In contrast, the post-
81 illumination rebound surge in $[K^+]_o$ following archaerhodopsin activation appears much smaller
82 than for halorhodopsin.
83
84 **Methods**
85 **Ethical Approval:** All procedures performed were in accordance with the guidelines of the
86 Home Office UK and Animals (Scientific Procedures) Act 1986 and approved by the Animal
87 Welfare and Ethical Review Body at both Newcastle University and UCL. Male and female mice
88 were used for experimentation.
89 **Archaerhodopsin viral injections:** C57/B6 adult mice were injected with AAV9.CAG.ArchT,
90 purchased from the UPenn vector core. For these adult injections, done at 8-12 weeks of age,
91 animals were anesthetized by ketamine–methoxamine intraperitoneal injection and placed in a
92 stereotaxic head holder (David Kopf Instruments). Injections were made at three to four
93 locations in an anterior–posterior row in one hemisphere, 1.5–2 mm lateral to the midline and
94 1–0.4 mm deep to the pia (0.6 µl, injected over 15 min).
95 **Slice Preparation:** We used both wild-type C57/B6 mice, and also mice expressing eNpHR3.0
96 within the pyramidal cell population, generated by cross-breeding homozygous Emx1-cre mice
97 (Jackson Laboratory, Stock 005628) with mice containing a floxed STOP cassette in front of an
98 eNpHR3.0/EYFP domain (Jackson Laboratory, Stock 014539; both maintained on the C57/B6
99 background). Emx1-promoter yields gene expression only in pyramidal cells in neocortex, in
100 adult mice, although it can drive gene in glia in other brain areas, and early in development
101 (Gorski et al., 2002). Experiments were performed on mice aged 1 - 8 months, of both sexes.
102 Mice were first decapitated, brains were removed and placed in cold cutting solution containing

103 (in mM): 3 MgCl2; 126 NaCl; 2.6 NaHCO3; 3.5 KCl; 1.26 NaH2PO4; 10 glucose. 400 µm
104 horizontal sections were made on a Leica VT1200 vibratome (Leica Microsystem, Germany).
105 Slices were stored at room temperature, in an interface holding chamber for 1 – 4 hours prior
106 to experimentation. Solutions were bubbled with carboxygen (95% O2 and 5% CO2) in artificial
107 cerebro-spinal fluid (aCSF) containing (in mM): 2 CaCl2; 1 MgCl2; 126 NaCl; 26 NaHCO3; 3.5 KCl;
108 1.26 NaH2PO4; 10 glucose.

109 ***In vitro* Extracellular recordings:** Extracellular recordings were performed using an interface
110 recording chamber. Slices were placed in the recording chamber perfused with either aCSF,
111 supplemented in different experiments with different combinations of the following drugs:
112 1µM Tetrodotoxin (TTX) (Abcam), 10mM tetraethylammonium (TEA) (Sigma), as indicated in
113 the results section. Recordings were obtained using aCSF-filled ~1-3MΩ borosilicate glass
114 microelectrodes (GC120TF-10; Harvard apparatus, Kent) placed in deep layers of neocortex.
115 Extracellular potassium $[K^+]_o$ was measured using single-barrelled K^+-selective microelectrodes.
116 The pipettes were pulled from nonfilamented borosilicate glass (Harvard Apparatus, Kent, UK),
117 and the glass was exposed to vapor of dimethyl-trimethyl-silylamine (Sigma-Aldrich), baking at
118 200^0 C for 40 minutes. The pipettes were then backfilled with aCSF. A short column of the K^+
119 sensor (Potassium ionophore I, cocktail B; Sigma-Aldrich, #99373) was taken into the tip of the
120 salinized pipette by using slight suction. The recordings through the K^+-sensor electrode were
121 referenced to a second electrode filled with aCSF. From the differential signal from a custom
122 build amplifier, we calculated the $[K^+]_o$ from calibration recordings made in an open bath, using
123 sudden increments in $[K^+]_o$. This provided a scaling factor S, of 55-59mV, where the K^+
124 concentration at a given moment in time, t, was calculated from the differential voltage, V(t), as
125 follows: $[K]_o = [K]_{o.baseline}\ 10^{V(t)/S}\ [K]_{o.baseline}$ for our experiments was 3.5 mM. The temperature of
126 the chamber and perfusate was maintained at 33-36 ℃ using a closed circulating heater
127 (FH16D, Grant instruments, Cambridge, UK). The solutions were perfused at the rate of 3
128 mls/min by a Watson Marlow 501U peristaltic pump (Watson-Marlow Pumps Limited, Cornwall
129 UK). For the collection of the HaloRhodopsin and ArchT data, the direct current local field
130 potential signal was unfiltered and amplified to a 10X output with a custom build amplifier.
131 These waveform signals were digitized with a Micro 1401-3 ADC board (Cambridge Electronic

132 Design, UK) and Spike2 version 7.10 software (Cambridge Electronic Design, UK). Signals were
133 sampled at 10 kHz. Recordings were analysed using a custom-written code in Matlab2015b
134 (Mathworks, MA, USA).

135 **Optogenetic illumination for extracellular recordings:** Optogenetic illumination was delivered
136 for 90s continuous periods, using a Fiber-coupled LED light at 565 nm (Thorlabs, M565F3) and
137 driven by an LED driver (Thorlabs, LEDD1) placed in trigger mode. Light output was measured at
138 an average of 9 mW. The LED light was positioned just above the superficial layers of the
139 neocortex for the slice experiments and pointed toward the deep layers, where the
140 extracellular recordings were performed.

141 **Statistics:** Statistical analysis of electrophysiology was performed using GraphPad Prism
142 (GraphPad Software, Inc., La Jolla, CA, USA). Data was analysed using Mann-Whitney test
143 (MATLAB, *ranksum.m*) or multiple linear regression modelling (*fitlm.m*). Figures of
144 electrophysiology traces were created in Matlab2015b or 2018b (Mathworks, MA, USA).

145 Results

146 Activation of archaerhodopsin causes secondary redistribution of K^+ ions

147 We previously reported that activation of the optogenetic chloride pump, halorhodopsin,
148 induced a secondary ionic redistribution of K^+ ions into the cell during the period of activation,
149 followed by a surge in $[K^+]_o$ after illumination ended (Parrish et al., 2023). The inward
150 movement of K^+ appears to pass through leak K^+ channels, whereas the post-illumination
151 outward movement included a KCC2-sensitive component, implying that it was driven in part by
152 the need to remove Cl^- ions that had been pumped into cells. We reasoned therefore that
153 these effects may be replicated in part by activation of other optogenetic pumps. To test this
154 prediction, we recorded the pattern of K^+ redistribution associated with activation of the proton
155 pump, archaerhodopsin (Figure 1). Widespread archaerhodopsin expression in the pyramidal
156 cell population was achieved by injecting a viral vector carrying the floxed gene into mice
157 expressing Cre-recombinase under the Emx1 promoter (Gorski et al., 2002). During periods of
158 illumination, we recorded a highly significant drop in $[K^+]_o$ in brain slices expressing

159 archaerhodopsin (Figure 1), but not in brain slices from wild-type mice. This K^+ redistribution
160 was almost entirely eliminated by blockade of plasmalemmal K^+ channels, using TEA. In both
161 respects, archaerhodopsin mimicked the effect we had previously reported in halorhodopsin-
162 expressing brain slices. In our preparations, the amplitude of the K^+ redistribution was larger in
163 the halorhodopsin-expressing brain slices, which might reflect the degree of hyperpolarization
164 achieved.

165 At the end of the illumination period, we previously reported that halorhodopsin-
166 expressing brain slices showed a very large rebound surge in $[K^+]_o$ (7.98 $\pm$ 0.41 (mean $\pm$ s.e.m),
167 range 5.5 - 10.6 mM; 95% confidence interval = 7.18 - 8.78 mM). In contrast, the post-
168 illumination surge in archaerhodopsin-expressing slices was significantly above the 3.5mM
169 baseline level (4.12 $\pm$ 0.12 mM, range 3.4 - 5.1 mM; 95% confidence interval = 3.86 - 4.38 mM),
170 but significantly smaller than occurred with the halorhodopsin slices (ArchT vs Halorhodopsin, p
171 = 0.0001, two-tailed Mann-Whitey test) (Figure 2).

172 For both opsins, a component of the rebound surge will be extrusion of K^+ ions that
173 moved into the neurons during the period of illumination; since the illumination-induced
174 inward movement was greater in our halorhodopsin group (possibly due to stronger
175 expression; during Halorhodopsin activation, the range of the drop in of drop in $[K^+]_o$ = 1.2 - 2.2
176 mM below baseline (3.5mM); during ArchT activation, the range = 0.5 – 1.3 mM below
177 baseline), one possibility is that the larger rebound in that group simply reflected this
178 difference. One approach to test this would have been to adjust expression patterns or
179 illumination levels to try to match the amplitude of the illumination-induced drop for the two
180 different opsins, but the halorhodopsin experiments were performed first, and we were not
181 able to achieve the same degree of K^+ redistribution with the archaerhodopsin. Instead, we
182 pooled the datasets and used multilinear regression modelling of the $[K^+]_o$, with the predictive
183 variables being the illumination-induced drop, and the type of opsin expressed, to assess their
184 relative contributions to the post-illumination surge (Table 1). We found no correlation
185 between the amplitude of the illumination-induced drop in $[K^+]_o$, and the rebound surge in $[K^+]_o$
186 for either experimental group individually (Table 1; Figure 3), whereas across the entire data
187 set, virtually all the variance was explained by the type of opsin, and almost nothing by the size

of the preceding, illumination-induced drop in $[K^+]_o$. This is consistent with our previous data showing that a large element of the post-illumination surge in halorhodopsin slices was sensitive to blockade of KCC2, indicating that the surge is boosted significantly by being coupled also to Cl^- extrusion in the halorhodopsin experiments.

A final point of difference is that in none of the archaerhodopsin experiments did we observe cortical spreading depolarization events; in contrast, these were triggered quite readily in halorhodopsin-expressing tissue (not illustrated, but examples are found in (Parrish et al., 2023)).

Discussion

Archaerhodopsin and halorhodopsin have both been used to inhibit neuronal activity, but do so by driving ionic movement in opposite directions: halorhodopsin by driving Cl^- inwards, and archaerhodopsin by driving H^+ out. We show here that this is further reflected by differences in the pattern of secondary effects, consistent with our interpretation of these effects reported in a previous study of halorhodopsin. The two optogenetic pumps share the effect of hyperpolarizing neurons, and consistent with this, both show a secondary drop in $[K^+]_o$, caused by K^+ moving into the stimulated cells through leak channels driven by the altered electro-chemical balance for K^+ during the period of opsin activity. The rebound, post-illumination surge in $[K^+]_o$, however, appeared much smaller for archaerhodopsin, even allowing for the fact that the expression levels of the two opsins were not exactly equivalent (halorhodopsin expression was achieved by cross-breeding Emx1 and floxed halorhodopsin mouse lines; archaerhodopsin expression was obtained by injecting Emx1 mice with a viral vector carrying the floxed archaerhodopsin gene) and so we were unable to achieve the same degree of K^+ loading during the periods of illumination. Across the entire dataset, pooled from both halorhodopsin- and archaerhodopins-expressing brain slices, virtually all the variance in the peak amplitude of the rebound $[K^+]_o$ was explained by the choice of opsin, and very little by the within-illumination drop.

The much larger rebound surge in $[K^+]_o$ with halorhodopsin is, in fact, in line with what can be predicted from the different actions of the two opsin pumps. Halorhodopsin loads the

216 cell with chloride, whereas archaerhodopsin consumes protons from the abundant intracellular
217 buffer species. Even if halorhodopsin and archaerhodopsin current amplitudes and durations
218 were identical, only halorhodopsin loads the cell with parallel inward fluxes of K^+ and Cl^-,
219 leading to outward transport of KCl by KCC2, which is an electroneutral transporter capable of
220 restoring a normal intraneuronal Cl^- level rapidly after a Cl^- load. This pattern of ionic
221 redistribution is consistent with previous observations that the rebound $[K^+]_o$ surge, following
222 chloride-loading arising either naturally, following intense GABAergic activation (Viitanen et al.,
223 2010), or artificially from halorhodopsin activation (Parrish et al., 2023), is reduced by blockers
224 of KCC2.

225 These collected observations, including the much smaller surge following
226 archaerhodopsin activation, further reinforces the view that $[Cl^-]_i$ and $[K^+]_o$ are tightly coupled,
227 as seen with the large rise in $[K^+]_o$ that follows intense interneuronal activation or direct GABA
228 application (Chang et al., 2018; Viitanen et al., 2010). These observations warrant a
229 reconsideration of the nature of raised $[K^+]_o$ during epileptic seizures, which may comfortably
230 exceed 10mM at its peak (Hablitz and Heinemann, 1987; Librizzi et al., 2017; Raimondo et al.,
231 2015; Somjen, 2004). This has often been attributed solely to K^+ movement out of cells during
232 action potentials, as described originally by Hodgkin and Huxley (Hodgkin and Huxley, 1952).
233 Recordings of the ictal initiation period typically also show a significant rise in $[K^+]_o$ ahead of the
234 time when pyramidal cells are recruited, as is readily apparent in published recordings (Chizhov
235 et al., 2022; Librizzi et al., 2017). Notably, this early peak coincides with a period of very intense
236 interneuronal activity (Parrish et al., 2019; Trevelyan et al., 2006). A major contribution to this
237 early rise, therefore, is likely to be the extrusion of K^+ coupled to Cl^--clearance, following a
238 period of significant chloride-loading due to intense GABAergic bombardment. Recognising
239 these two different causes of K^+ extrusion – (1) the Hodgkin-Huxley model of action potential
240 firing and (2) coupled to the clearance of Cl^- is important to our understanding of ictal
241 propagation and recruitment to seizures (Graham et al., 2022; Trevelyan et al., 2022).

242 The most surprising secondary effect triggered by prolonged halorhodopsin activation
243 was the occurrence of CSDs, at times, arising from a state where the majority of neurons were
244 hyperpolarized to different degrees, and $[K^+]_o$ was below baseline levels (Parrish et al., 2023).

245 We did not observe such events in our archaerhodopsin preparations. Two possible
246 explanations suggest themselves for this difference, both consistent with our data: first that the
247 lack of CSDs in our archaerhodopsin experiments reflects the smaller shifts in K^+ (Figure 3), or
248 second that it reflects differences in the net ion flux during illumination. Halorhodopsin
249 activation results in both inward Cl^- and K^+ movement, generating a large net influx of
250 osmotically active particles. In contrast, archaerhodopsin drives an outward proton movement,
251 and the K^+ redistribution is much smaller. While this negative finding (no CSDs in our
252 archaerhodopsin experiments) represents a limited test of the hypothesized differences
253 between halorhodopsin and archaerhodopsin, the result is consistent with what else is known
254 about their different mechanisms of action.
255

256 ## Figure and Table Legends

257 **Figure 1. The main movement of K^+ ions from the extracellular space, induced by opsin**
258 **activation is through K^+ channels.**
259 (A) Redistribution of K^+, assessed by recording $[K^+]_o$ during a period of halorhodopsin (black) or
260 of archaerhodopsin activation (red) in the presence of TTX to block neuronal firing, and
261 additionally TEA to block "leak" K^+ channels. (B) Pooled data of measurements of $[K^+]_o$ for all
262 the halorhodopsin and archaerhodopsin recordings. For both opsins, the size of the K^+
263 redistribution is greatly reduced by block of voltage-gated K^+ channels (Halo vs Halo + TEA, p =
264 0.00076; Arch vs Arch + TEA, p = 0.0279, two-tailed Mann-Whitney test).

265 **Figure 2. The large post-illumination surge in $[K^+]_o$ following a period of halorhodopsin**
266 **activation is not replicated by archaerhodopsin activation.**
267 (A) Recordings of extracellular $[K^+]$ in brain slices in which either Halorhodopsin (blue, top), or
268 Archaerhodopsin (red, middle), was expressed in all pyramidal cells, or in a slice with no opsin
269 expression (black, bottom). Yellow bar represents the time of illumination (90s period). Light
270 activation of Halorhodopsin induced a very marked reduction in $[K^+]_o$, followed by an even
271 larger, rebound increase. There was also a drop in $[K^+]_o$, synchronous with activation of
272 Archaerhodopsin, but the rebound was negligible. Brain slices without opsins showed no light
273 induced fluctuations in $[K^+]_o$. (B) The peak extracellular $[K^+]$, after the end of illumination, for
274 Archaerhodopsin (mean peak = 4.12mM, n = 11) and Halorhodopsin activation (mean peak =
275 7.98mM; n = 15; comparison, p = 0.0001, two-tailed Mann-Whitey test), respectively.
276

277 **Figure 3. The post-illumination $[K^+]_o$ rise does not reflect the drop in $[K^+]_o$ during illumination.**
278 A plot of the $[K^+]_o$ rise, in excess of baseline (3.5mM), following the end of illumination versus
279 the drop in $[K^+]$o below baseline that occurs during illumination for 25 different brain slices, 14
280 expressing Halorhodopsin (red) and 11 expressing Archaerhodopsin-T (black). Halorhodopsin
281 activation, using the expression systems available to us, produced a larger K^+ dip during
282 illumination (range 1.2-2.2mM below baseline) than did activation of ArchT (0.5-1.3mM below
283 baseline). The dotted lines represent the correlation for the two experimental groups,

extended to the ordinate axis. The difference in the intercepts represents the effect of chloride loading, secondary to halorhodopsin activation, producing an excess return of K^+ to the extracellular space. Table 1 shows the R^2 values for different linear regression models, which show that virtually all the experimental variation is explained in terms of the two experimental groups, and almost none by the intra-illumination $[K^+]_o$ drop.

Table 1. Linear regression model analyses of Archaerhodopsin and Halorhodopsin $[K^+]_{extra}$. Linear regression model analyses of the data presented in Figure 3, examining different models of the post-illumination rise in $[K^+]_{extra}$ predicted by the expression of either Halorhodopsin or ArchT, and the degree of $[K^+]_{extra}$ drop during the period of illumination. The 3rd analysis ("$[K^+]$ drop (all)") is of the dataset with ArchT and Halorhodopsin brain slices pooled together without distinction. This distinction is made in the 4th analysis (("$[K^+]$ drop, ArchT/Halo grouped"), whereas the 5th analysis does not include information about the $[K^+]$ drop during illumination. Note that the adjusted R^2 actually improves without the $[K^+]$ drop information, indicating that the post-illumination $[K^+]$ rise is explained almost solely by the difference between the opsins.

References

Alfonsa, H., Merricks, E.M., Codadu, N.K., Cunningham, M.O., Deisseroth, K., Racca, C., and Trevelyan, A.J. (2015). The contribution of raised intraneuronal chloride to epileptic network activity. J Neurosci *35*, 7715-7726.

Boyden, E.S., Zhang, F., Bamberg, E., Nagel, G., and Deisseroth, K. (2005). Millisecond-timescale, genetically targeted optical control of neural activity. Nat Neurosci *8*, 1263-1268.

Chang, M., Dian, J.A., Dufour, S., Wang, L., Moradi Chameh, H., Ramani, M., Zhang, L., Carlen, P.L., Womelsdorf, T., and Valiante, T.A. (2018). Brief activation of GABAergic interneurons initiates the transition to ictal events through post-inhibitory rebound excitation. Neurobiol Dis *109*, 102-116.

Chizhov, A.V., Amakhin, D.V., Smirnova, E.Y., and Zaitsev, A.V. (2022). Ictal wavefront propagation in slices and simulations with conductance-based refractory density model. PLoS Comput Biol *18*, e1009782.

Chow, B.Y., Han, X., Dobry, A.S., Qian, X., Chuong, A.S., Li, M., Henninger, M.A., Belfort, G.M., Lin, Y., Monahan, P.E.*, et al.* (2010). High-performance genetically targetable optical neural silencing by light-driven proton pumps. Nature *463*, 98-102.

Deisseroth, K. (2015). Optogenetics: 10 years of microbial opsins in neuroscience. Nat Neurosci *18*, 1213-1225.

Gorski, J.A., Talley, T., Qiu, M., Puelles, L., Rubenstein, J.L., and Jones, K.R. (2002). Cortical excitatory neurons and glia, but not GABAergic neurons, are produced in the Emx1-expressing lineage. J Neurosci *22*, 6309-6314.

Graham, R.T., Parrish, R.R., Alberio, L., Johnson, E.L., Owens, L., and Trevelyan, A.J. (2022). Optogenetic stimulation reveals a latent tipping point in cortical networks during ictogenesis. Brain.

Hablitz, J.J., and Heinemann, U. (1987). Extracellular K+ and Ca2+ changes during epileptiform discharges in the immature rat neocortex. Brain Res *433*, 299-303.

Hodgkin, A.L., and Huxley, A.F. (1952). Currents carried by sodium and potassium ions through the membrane of the giant axon of Loligo. J Physiol *116*, 449-472.

Kaila, K., Price, T.J., Payne, J.A., Puskarjov, M., and Voipio, J. (2014). Cation-chloride cotransporters in neuronal development, plasticity and disease. Nat Rev Neurosci *15*, 637-654.

Librizzi, L., Losi, G., Marcon, I., Sessolo, M., Scalmani, P., Carmignoto, G., and de Curtis, M. (2017). Interneuronal Network Activity at the Onset of Seizure-Like Events in Entorhinal Cortex Slices. J Neurosci *37*, 10398-10407.

Parrish, R.R., Codadu, N.K., Mackenzie-Gray Scott, C., and Trevelyan, A.J. (2019). Feedforward inhibition ahead of ictal wavefronts is provided by both parvalbumin- and somatostatin-expressing interneurons. J Physiol *597*, 2297-2314.

Parrish, R.R., MacKenzie-Gray Scott, C., Jackson-Taylor, T., Grundmann, A., McLeod, F., Codadu, N.K., Calin, A., Alfonsa, H., Wykes, R.C., Voipio, J.*, et al.* (2023). Indirect Effects of Halorhodopsin Activation: Potassium Redistribution, Nonspecific Inhibition, and Spreading Depolarization. J Neurosci *43*, 685-692.

Raimondo, J.V., Burman, R.J., Katz, A.A., and Akerman, C.J. (2015). Ion dynamics during seizures. Frontiers in cellular neuroscience *9*, 419.

Raimondo, J.V., Kay, L., Ellender, T.J., and Akerman, C.J. (2012). Optogenetic silencing strategies differ in their effects on inhibitory synaptic transmission. Nat Neurosci *15*, 1102-1104.

Rivera, C., Voipio, J., Payne, J.A., Ruusuvuori, E., Lahtinen, H., Lamsa, K., Pirvola, U., Saarma, M., and Kaila, K. (1999). The K+/Cl- co-transporter KCC2 renders GABA hyperpolarizing during neuronal maturation. Nature *397*, 251-255.

Somjen, G.G. (2004). Ions in the brain: Normal function, seizures and stroke (Oxford: Oxford University Press).

Trevelyan, A.J., Graham, R.T., Parrish, R.R., and Codadu, N.K. (2022). Synergistic positive feedback mechanisms underlying seizure initiation. Epilepsy Currents.

Trevelyan, A.J., Sussillo, D., Watson, B.O., and Yuste, R. (2006). Modular propagation of epileptiform activity: evidence for an inhibitory veto in neocortex. J Neurosci *26*, 12447-12455.

Viitanen, T., Ruusuvuori, E., Kaila, K., and Voipio, J. (2010). The K+-Cl cotransporter KCC2 promotes GABAergic excitation in the mature rat hippocampus. J Physiol *588*, 1527-1540.

Zhang, F., Wang, L.P., Brauner, M., Liewald, J.F., Kay, K., Watzke, N., Wood, P.G., Bamberg, E., Nagel, G., Gottschalk, A.*, et al.* (2007). Multimodal fast optical interrogation of neural circuitry. Nature *446*, 633-639.

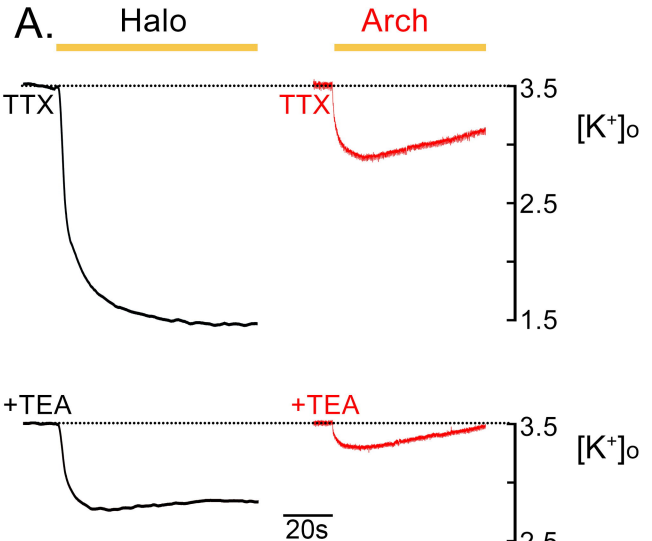
A.
Halo
Arch
TTX
TTX
3.5
2.5
1.5
[K+]o
+TEA
+TEA
3.5
2.5
[K+]o
20s

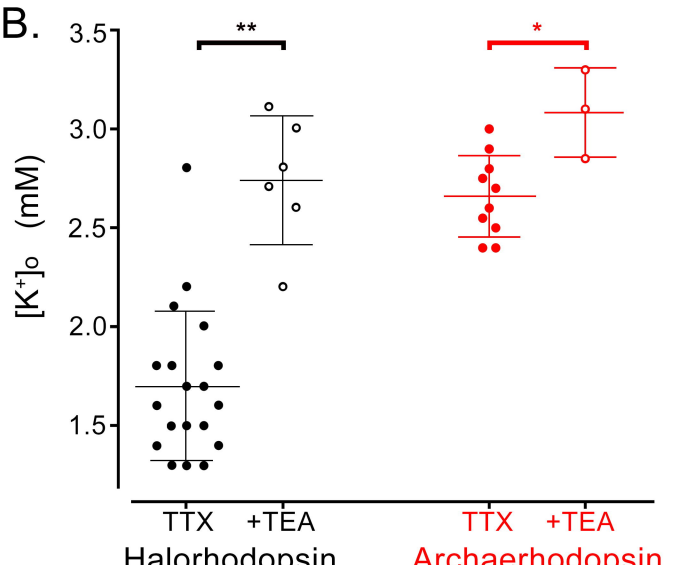
B.
**
*
3.5
3.0
2.5
2.0
1.5
[K+]o (mM)
TTX
+TEA
TTX
+TEA
Halorhodopsin
Archaerhodopsin

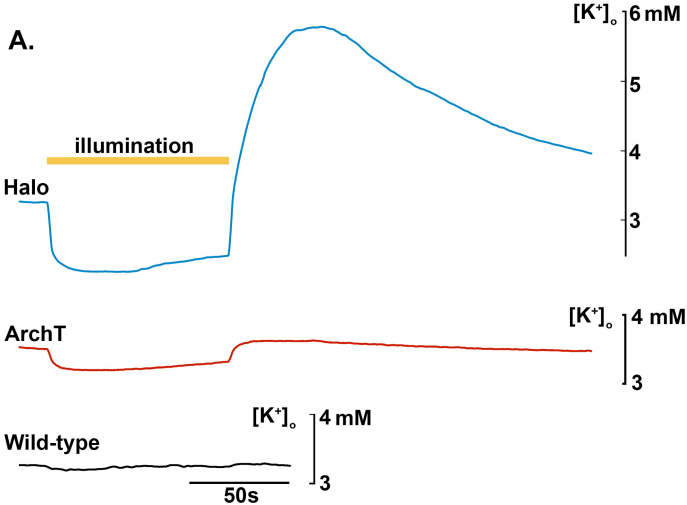
A.
illumination
Halo
[K+]o
6 mM
5
4
3
ArchT
[K+]o
4 mM
3
Wild-type
[K+]o
4 mM
3
50s

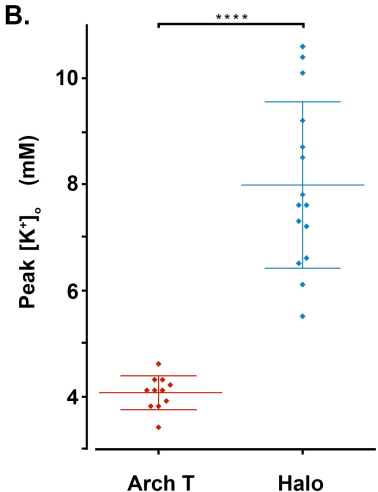
B.
****
Peak [K+]o (mM)
10
8
6
4
Arch T
Halo

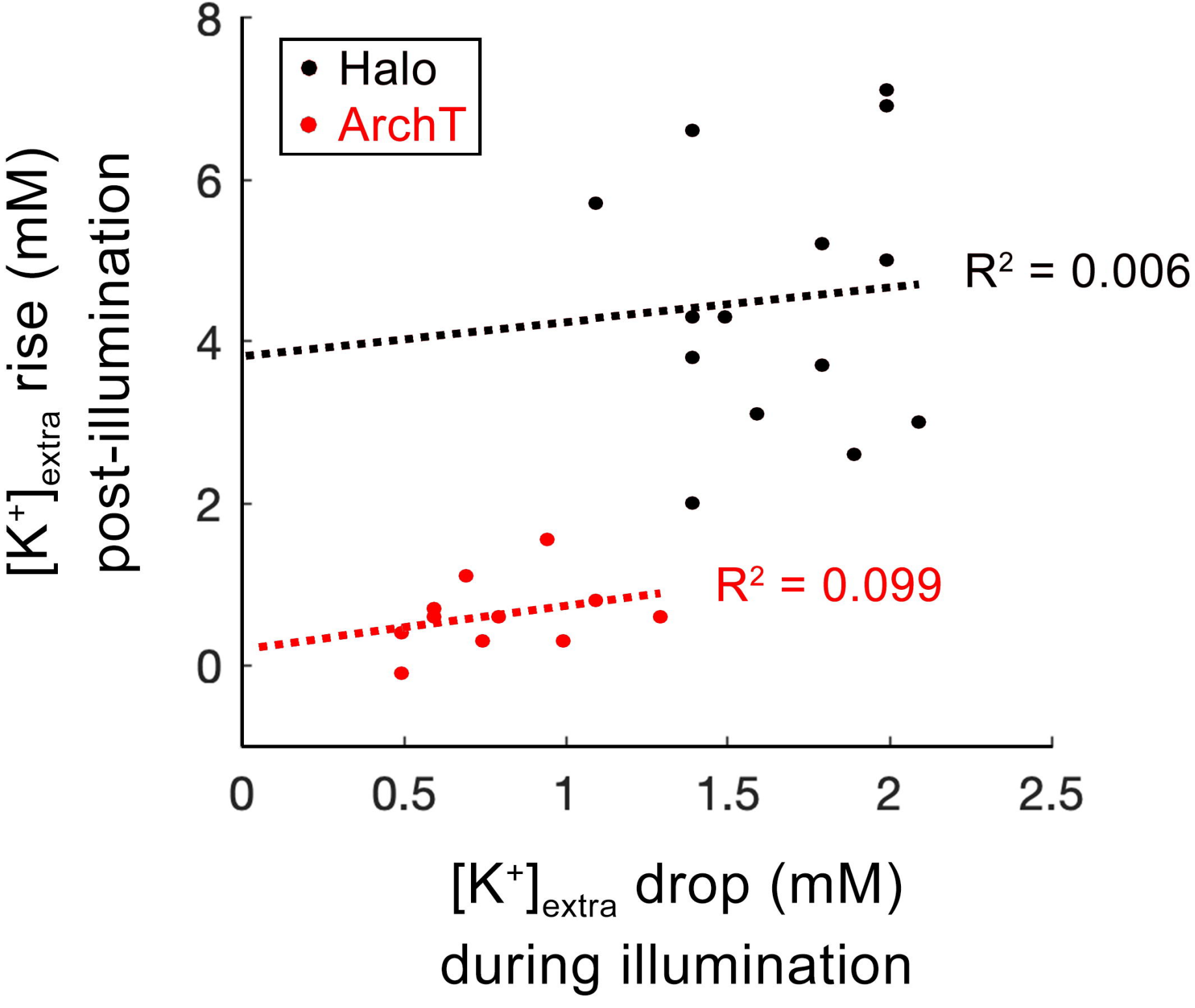
Halo
ArchT
R^2 = 0.006
R^2 = 0.099
8
6
4
2
0
0
0.5
1
1.5
2
2.5
$[K^+]_{extra}$ rise (mM)
post-illumination
$[K^+]_{extra}$ drop (mM)
during illumination

Table 1. Models

		R^2	Adjusted R^2	p value
$[K^+]$ rise vs	$[K^+]$ drop (Halo)	0.006	-0.076	0.79
	$[K^+]$ drop (ArchT)	0.099	-0.001	0.35
	$[K^+]$ drop (all)	0.554	0.535	$< 10^{-4}$
	$[K^+]$ drop, ArchT/Halo grouped	0.724	0.699	$< 10^{-6}$
	ArchT/Halo grouped	0.721	0.709	$< 10^{-7}$